Geoscience Frontiers 13 (2022) 101277

Contents lists available at ScienceDirect

Geoscience Frontiers

journal homepage: www.elsevier.com/locate/gsf

Research Paper

Ultrasonic prediction of crack density using machine learning: A numerical investigation

Sadegh Karimpouli [a,*], Pejman Tahmasebi [b], Erik H. Saenger [c,d,e]

[a] Mining Engineering Group, Faculty of Engineering, University of Zanjan, Zanjan, Iran
[b] Department of Petroleum Engineering, University of Wyoming, Laramie, WY 82071, USA
[c] Bochum University of Applied Sciences, 44801 Bochum, Germany
[d] Fraunhofer IEG, Fraunhofer Research Institution for Energy Infrastructure and Geothermal Systems, 44801 Bochum, Germany
[e] Ruhr-University Bochum, 44801 Bochum, Germany

ARTICLE INFO

Article history:
Received 12 April 2021
Revised 8 July 2021
Accepted 22 July 2021
Available online 24 July 2021
Handling Editor: M. Santosh

Keywords:
Machine learning
Crack density
Ultrasonic wave
Numerical computation

ABSTRACT

Cracks are accounted as the most destructive discontinuity in rock, soil, and concrete. Enhancing our knowledge from their properties such as crack distribution, density, and/or aspect ratio is crucial in geo-systems. The most well-known mechanical parameter for such an evaluation is wave velocity through which one can qualitatively or quantitatively characterize the porous media. In small scales, such information is obtained using the ultrasonic pulse velocity (UPV) technique as a non-destructive test. In large-scale geo-systems, however, it is inverted from seismic data. In this paper, we take advantage of the recent advancements in machine learning (ML) for analyzing wave signals and predict rock properties such as crack density (CD) – the number of cracks per unit volume. To this end, we designed numerical models with different CDs and, using the rotated staggered finite-difference grid (RSG) technique, simulated wave propagation. Two ML networks, namely Convolutional Neural Networks (CNN) and Long Short-Term Memory (LSTM), are then used to predict CD values. Results show that, by selecting an optimum value for wavelength to crack length ratio, the accuracy of predictions of test data can reach $R^2 > 96\%$ with mean square error (MSE) < 25e-4 (normalized values). Overall, we found that: (i) performance of both CNN and LSTM is highly promising, (ii) accuracy of the transmitted signals is slightly higher than the reflected signals, (iii) accuracy of 2D signals is marginally higher than 1D signals, (iv) accuracy of horizontal and vertical component signals are comparable, (v) accuracy of coda signals is less when the whole signals are used. Our results, thus, reveal that the ML methods can provide rapid solutions and estimations for crack density, without the necessity of further modeling.

1. Introduction

Cracks (and fractures) are one of the most well-known destructive features of rocks, soil and concrete decreasing their strength and causing instabilities in geo-systems. They are mostly induced due to a relief of in-situ stresses and/or changing of other environmental factors such as pressure, temperature, and precipitation, for example, during weathering. Their effects have been studied in a verity of fields such as civil and mining engineering (e.g., concrete and pavement characterization, slope stability, blasting, tunneling, and coal-bed methane mining) (Jing and Hudson, 2002; Hoek and Martin, 2014; Prasanna et al., 2016; Karimpouli et al., 2020a, 2020b; Rezanezhad et al., 2019; Zhang et al., 2021b), hydrocarbon and geothermal exploration (e.g., reservoir characterization, rock physics inversion, and hydraulic fracturing) (Hou et al., 2019; Bai and Tahmasebi, 2020, 2021; Kamali and Ghassemi, 2020; Karimpouli et al., 2013; van der Voet et al., 2020; Zhuang et al., 2020), image enhancement for complex microstructures (Kamrava et al., 2019), and even material science (e.g., microstructure characterization) (Blackshire, 2017). A comprehensive review of the advances and applications of machine learning in geosciences and geo-materials can be found elsewhere (Tahmasebi et al., 2020). Also, Bayar and Bilir (2019) presented a comprehensive literature survey in crack detection methods in a variety of image types from X-ray tomography and digital photos to radar images using image processing and machine learning (ML) algorithms. For more info, see Bayar and Bilir (2019) and references therein.

* Corresponding author.
E-mail address: s.karimpouli@znu.ac.ir (S. Karimpouli).

https://doi.org/10.1016/j.gsf.2021.101277
1674-9871/

It has been shown that evaluation of crack density (CD), defined as the number of cracks per unit volume, is highly essential to better understand the behavior of geo-materials. The CD is not, however, an easy-to-measure parameter and is indirectly estimated either qualitatively or quantitatively from limited data. Visual inspection is a common method for evaluation of CD from conventional cameras and microscopic images or even from Scanning Electron microscopy images. Nasseri et al. (2007) microseismic events are the other source of data, which are induced due to fracturing and rock damage as the rock mass is brought to failure under high stress (Cai et al., 2001). Cai et al. (2001) monitored microseismic events near an excavation and represented them as fracture density of the rock mass. Other widely accepted methods are based on propagating elastic wave through rock samples and velocity measurement with the ultrasonic pulse velocity (UPV) technique. These measurements are then inverted into CD using the theory of wave propagation in porous media which was introduced by Biot (Biot, 1962, 1956) and Gassmann (Gassmann, 1951), which is known as Biot-Gassmann theory (Thomsen, 1985) and extended afterward. Although this theory is widely accepted for inversion of the velocity of porous rocks, it is not consistent with low porosity cracked-rocks. Therefore, other derivatives, namely Biot-Consistent (Thomsen, 1985) and Self-Consistent (Budiansky, 1965; Hill, 1965) theories, were extended to characterize the effects of cracks. Some other poroelasticity models were introduced to capture fluid effects on the cracked rocks (Ba et al., 2017; Zhang et al., 2019, 2020). Byun et al. (2015) used the Biot-Consistent theory and predicted CD of cracked-rocks using wave velocities obtained from lab tests. They found that compressional wave velocity and shear modulus of grains are the most sensitive parameters in this equation. Kachanov (1993) developed the Self-Consistent theory for cracks and pores in a specific effective medium (CPEM) to be applied in rocks with cracks. Based on this formulation, Schubnel et al. (2006) and Nasseri et al. (2007) inverted CD of rock from elastic wave velocities using a least-square technique. Although they showed that it is possible to conduct such an inversion simply, numerical studies by Orlowsky et al. (2003) and Saenger et al. (2004) revealed that Differential Effective Medium (Berryman, 1992) theory is the most suitable scheme for cracked-rocks. In a recent study, Yoon (2020) combined both Biot-Consistent and CPEM formulations and derived CD and crack aspect ratio in some artificially weathered rocks. Clearly, all these methods are affected by analytical limitations and simplifications. For example, the anisotropy of a real rock medium, and the aspect ratio, shape, and distribution of real cracks, are not fully considered in such analytical studies.

Machine Learning (ML) based methods are accounted as powerful and intelligent methods, which have been widely used for estimation, classification, and clustering. Recent advancements in deep computing showed that ML-based methods are applicable in many fields of sciences from machine vision (Nasirahmadi et al., 2019), medical imagery (Bernal et al., 2019) to even geosciences (Waldeland et al., 2018; Xiong et al., 2018; Karimpouli et al., 2020b; Kamrava et al., 2020; Karimpouli and Tahmasebi, 2020; Tang et al., 2021). This study aims to investigate the capability of these methods for the estimation of CD from waveform instead of simple wave velocity. Thus, we consider a digital model with a range of CD and then simulate the UPV test using rotated staggered finite-difference grid (RSG) technique (Saenger and Shapiro, 2002) to numerically compute waveform signal, which could be transmitted, reflected, or even coda waves. Such a signal can be regarded as a 1-dimensional (1D) input array for ML networks. 1D data have been used for many other purposes such as speech recognition (Zhang et al., 2017), seismic signal processing (Duan and Zhang, 2020), and earthquake applications (e.g., for earthquake detection, phase picking, and early warning) (Mousavi et al., 2020; Zhang et al., 2021a). There are many types of ML networks that could be used for such a purpose (e.g., Bilir et al., 2016). Among them, Convolutional Neural Networks (CNN) (Krizhevsky et al., 2017) and Long Short-Term Memory (LSTM) (Hochreiter and Schmidhuber, 1997) are two well-known and highly beneficial networks, which are used in this study. CNNs extract high-order feature vectors of the input signal based on small convolutional kernels and translate them into the output using a Fully Connected Network (FCN). For example, Saenger et al. (2021) showed that CNNs are capable to be trained for prediction of damage zone characteristics of concrete using Coda waves. However, LSTMs belong to the group of recurrent networks, which selectively remember patterns for long durations of time and predict the output accordingly. Results from laboratory measurements have revealed that the nonlinearity of the acoustic signal (from UPV) increases by rising CD in both rock and concrete (Kim et al., 2020). Thus, it is theoretically understood that ML methods are able to capture such a relationship and produce reliable predictions for unseen cases, however, it has been tested neither numerically nor experimentally. The main objective of this paper is to evaluate the performance of ML methods for prediction CD from acoustic signals. From an application point of view, it would be beneficial if ML methods could be trained by 1D signals for such predictions. However, we aim to answer: (1) Which method (CNN or LSTM) does performs better? (2) What kind of acoustic waves (either transmitted or reflected waves) are the most appropriate waves for this problem and (3) Are Coda waves capable to be used for this purpose?

2. Methodology

2.1. Numerical modeling and data

Coda waves are considered to be the result of multiple scattering of seismic waves at material heterogeneities (Herraiz and Espinosa, 1987). For material characterization, body as well as surface waves are playing a particularly important role in this interaction. Therefore, coda waves provide a seismographic fingerprint of the material heterogeneities. Coda waves provide decisive information about the mechanisms of scattering and attenuation. One goal of this paper is to analyze this mechanism for predicting the effective elastic properties of cracked media induced by CD using ML.

A rotated staggered-grid (RSG) finite-difference scheme (Saenger et al., 2000) is used to propagate the seismic wavefield in the forward simulations. The RSG uses rotated finite-difference operators, leading to a distribution of modelling parameters in an elementary cell where all components of one physical property are located only at one single position. This can be advantageous for modelling wave propagation in anisotropic media or complex media, including high-contrast discontinuities because no averaging of elastic moduli is needed. Coda wave modelling is therefore a possible application of this technique. With regard to previous studies (Saenger and Shapiro, 2002; Krüger et al., 2005), we demonstrated that the RSG-technique is well-suited and accurate for this purpose.

The cracked region is filled with randomly orientated cracks. For the models with non-intersecting cracks the same procedure as in Saenger and Shapiro (2002) is used: if two cracks intersected during random selection, the more recent crack is eliminated and a random choice is made again. For the definition of the CD parameter, we use (Kachanov, 1992):

$$\mathrm{CD} = \frac{1}{A}\sum_{k=1}^{n} l_k^2 \tag{1}$$

where $2l_k$ is the length of rectilinear cracks, n is the number of cracks and A is the representative area. Fig. 1 left-hand side shows a typical model with CD = 0.3. The full model contains 1000 × 4000 grid-points with an interval of 0.00005 m. For the homogeneous background we set V_P = 5100 m/s, V_S = 2944 m/s and ρ_g = 2500-kg/m^3, while for the dry cracks we set V_P = 0 m/s, V_S = 0 m/s and ρ_g = 0.0001 kg/ m^3, which approximates a vacuum. Thus, each additional crack increases the porosity.

We perform our modelling experiments with periodic boundary conditions in the horizontal direction. For this reason, our elastic models are also generated with this periodicity. Hence, it is possible for a single crack to start at the right side of the model and to end at its left side. To obtain the seismograms in different models we apply a body force line source at the top of the model. The plane wave generated in this way propagates in a downward direction through the fractured medium (Fig. 1). A finite-difference operator of second order is used in time as well as in space. The source wavelet in our experiments is always the first derivative of a Gaussian, with different dominant frequencies, and with a time increment Δt = 2.1 × 10^{-9} s. With two horizontal lines of receivers at the top (depth = 0.00005 m) and in the bottom of cracked region (depth = 1001 × 0.00005 m), top and bottom receivers in Fig. 1, it is possible to record the mean peak amplitude of the plane wave and the coda waves caused by the inhomogeneous region. The top and bottom receiver lines will record mainly reflected waves and transmitted waves, respectively. These receivers are set to record wave point movements in x- and z-direction individually, known as x- and z-components in this study (Fig. 1). The receiver lines make it possible to record wave movement in 2D section (time-distance), which we call them 2D signals. Thus, each 2D signal could be in x- or z-component (Fig. 1). To generate 1D signals, we compute an average signal of all receivers in a line as shown in Fig. 1.

A typical simulation with a model size of 5 cm × 20 cm consists of 4 million grid points and a simulation with 40,000 time steps takes about 5 min on one node of a mid-size cluster computer. >10,000 simulations are performed for this study with different CDs (0.1, 0.2, 0.3 and 0.4), wavelengths (0.0127, 0.051 and 0.204 m) and crack length (0.15, 0.5 and 2 mm). For example, Figs. 2 and 3 show 2D and 1D transmitted signals, respectively, in both x- and z-components with a wavelength of 0.0127 m and different CDs of 0.1, 0.2, 0.3 and 0.4. According to these figures, different patterns are generated by different CDs, which are theoretically suitable for intelligent methods to capture their complex relations. In the z-component, the high amplitude signal shows arrival of the plane wave. Clearly, the arrival time depends on the CD value and is accounted as an informative attribute for the ML methods to learn the relation. We generate new signals by removing these

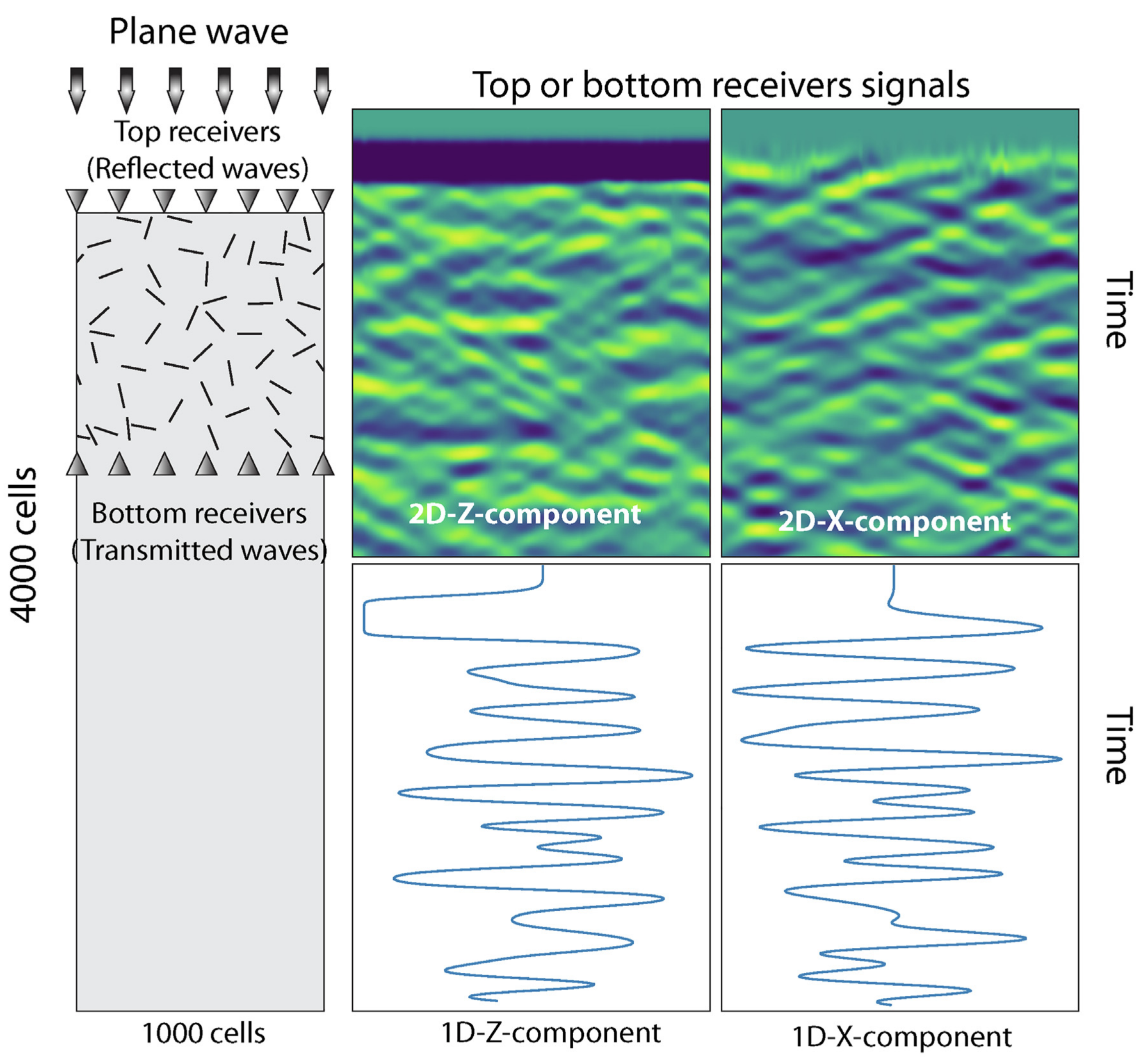

Fig. 1. Model configuration and various generated data.

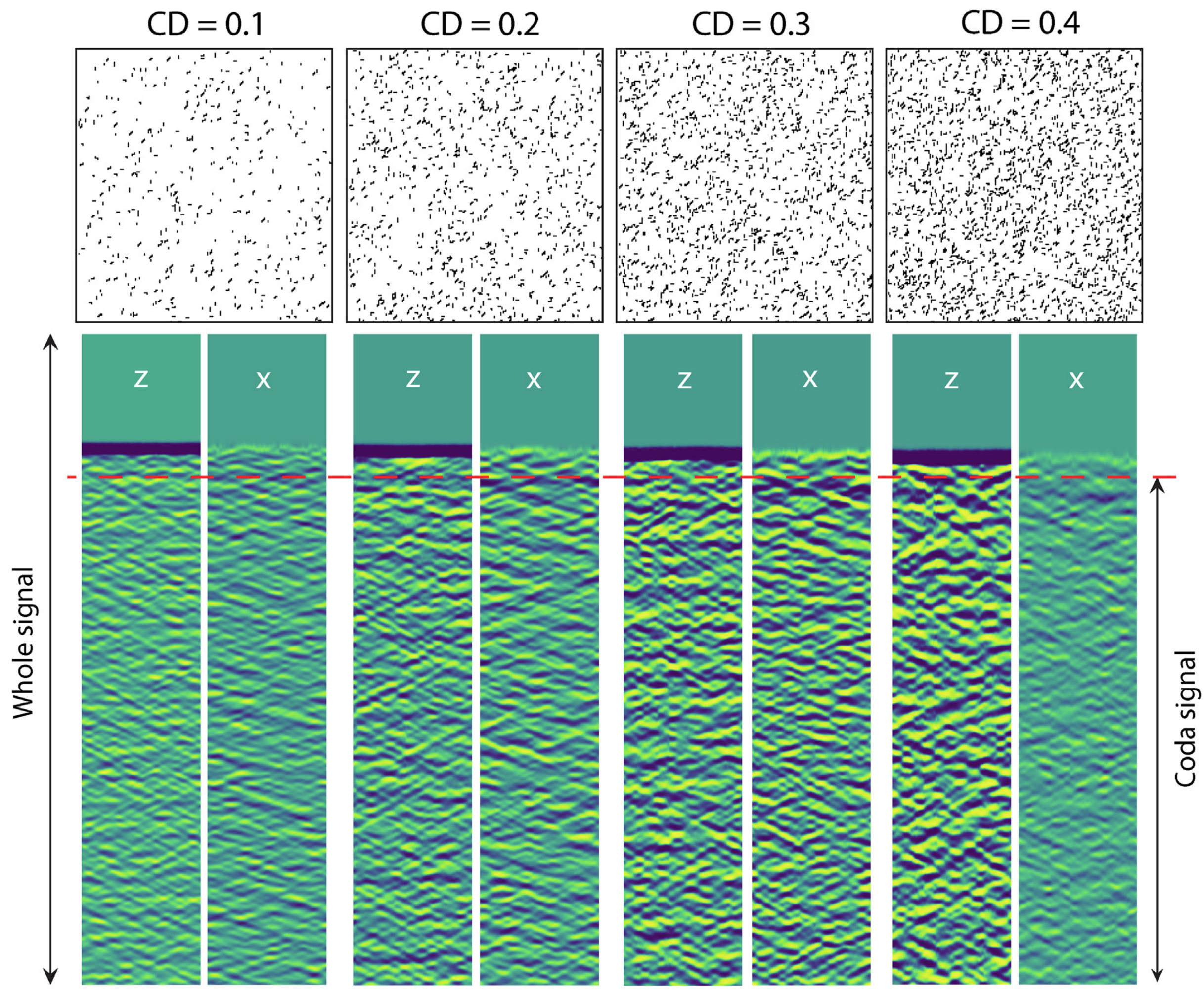

Fig. 2. 2D transmitted signals in *z*- and *x*-directions and corresponding coda signals with wavelength of 0.0127 m and different CDs of 0.1, 0.2, 0.3 and 0.4.

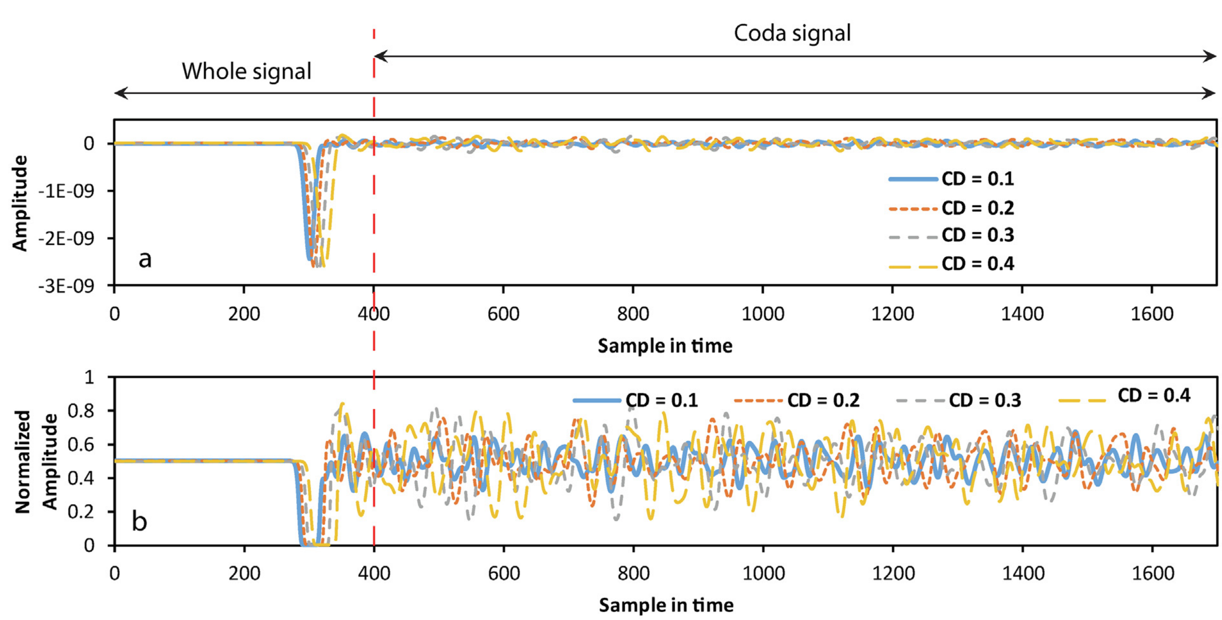

Fig. 3. (a) Simulated and (b) normalized 1D transmitted and coda signals in *z*-direction with a wavelength of 0.0127 m and different CDs of 0.1, 0.2, 0.3 and 0.4.

high amplitudes known as *the coda signal* (Figs. 2 and 3). The idea behind is to find the ML performance just based of perturbations caused by cracked region.

Please note, due to an integration-effect of the line source the wave-induced at the top is Gaussian-shaped with a high low-frequency content (in contrast to the first derivative of a Gaussian of the source). Strictly speaking, the wavelength used in this paper is an upper bound of 90% of the corresponding frequencies (because the wavelength was calculated with the corresponding fundamental frequency of the source wavelet). To find the effect of crack length and wavelength on the generated signals, we define wl/cl as wavelength to crack length ratio for each model and produce the signals accordingly. Fig. 4 shows 1D transmitted signals in *z*-direction with CD of 0.2 and different wl/cl = 0.64, 2.5, 8.5, 34 and 136. It is obvious that by increasing of wl/cl ratio a smoother signal is generated. During our investigation we will introduce some optimum ranges for wl/cl with more reliable predictions.

2.2. Machine learning methods

In this study, to find a robust and efficient method, two ML networks are used: the CNN and LSTM. These methods are extensively discussed elsewhere (Lecun et al., 1998; Krizhevsky et al., 2017; Aloysius and Geetha, 2018; Yu et al., 2019). However, a brief review of them is firstly introduced and, then, their specific architectures, used in this study, are presented. Our networks have been implemented in *Python* using *Keras* interface (based on *Tensorflow* platform) and, therefore, layers are named accordingly.

2.2.1. Architecture of the CNNs

The CNNs are composed of two main parts: feature extraction and conventional neural network. In the feature extraction part, small size kernels are convolved with the data and the results are activated using an activation function such as ReLU (Nair and Hinton, 2010). This leads to extract new features in a number of channels called convolutional layers. These layers are then downsampled through a moving window selecting either minimum, average or maximum values to produce features maps (or, in 1D, feature vectors). The extracted and downsampled features are used as the input layer of the conventional neural network part, which makes a connection between features and the output layer. The basic relation between one layer and the next is written as:

$$\mathbf{Y} = \left(\sum_i \mathbf{W}_i * \mathbf{X}_i\right) + \mathbf{b} \tag{2}$$

where $\mathbf{W}$ is the kernel (or weight matrix) and $\mathbf{X}$ is the input image (or last layer) each with i channels. $\mathbf{b}$ is the bias vector and $*$ is either convolution operation or dot product in convolutional layers and hidden layers. The CNN uses an optimization function such as *adam* (Kingma and Ba, 2014), trying to minimize a loss function such as *mean square errors (MSE)*, which is a criterion for difference between measured observations and estimation of the network. During the training phase, all connecting weights are optimized as the CNN could produce valid estimations for new data (e.g., test data).

There are many well-known CNN architectures for different purposes (Aloysius and Geetha, 2018), but here we designed specific architectures, which are best performed for our data. Table 1 reports the main features of all CNNs in this study. The general architecture used for all data are very similar, but there are also minor differences. For example, as it is reported in Table 1, the CNN used for 1D-transmitted waves contain 4 convolutional layers with 16, 32, 64, and 128 channels. Each of these layers are convolved with a kernel size of 9, 7, 5 and 3. They are followed by a Maxpooling layer with a pool size of 2, 10% Dropout layer and Bachnormalization. The downsampled features are transformed to the output (CD) using two Dense layers with 1024 and 1 channels. The '*Tanh*' and '*Sigmoid*' activation functions are used in Dense layers. In all networks, *adam* optimization function with a learning rate of 0.01 and *MSE* loss function is used. In some cases, we decreased the learning rate into 0.001.

2.2.2. Architecture of LSTM

When data from a sequence, for example in a sentence where every word or data depends on the previous ones, all previous inputs have to be considered for predicting the output. Traditional neural networks are designed to only use the data without considering the connection between them, while, in some cases such as this study, we need a network that can take the relationships between the input data into account while producing the output. Recurrent neural networks are designed to address this issue. When the sequence of data is short, such as a simple sentence, the recurrent neural networks (RNN) perform finely. However, a special type of RNN called long short-term memory (LSTM) performs more efficiently when the sequence becomes longer. In fact,

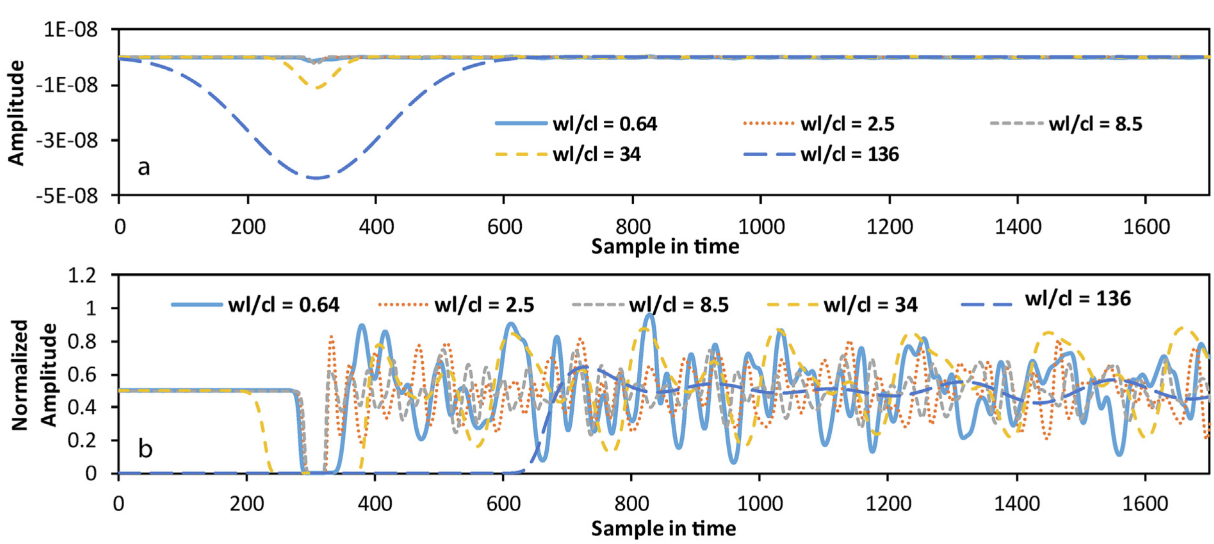

Fig. 4. (a) Simulated and (b) normalized 1D transmitted signals in z-direction with CD of 0.2 and different wl/cl = 0.64, 2.5, 8.5, 34 and 136.

Table 1
The architecture of the CNNs used in this study (ch: number of channels; k: kernel size; ReLU-, Tanh-, Sigmoid: activation functions).

Input layer	2D transmitted waves	1D transmitted waves	1D transmitted coda waves	1D reflected waves	1D transmitted coda waves
Conv(2D or 1D)	32 ch, 9 × 9 k, ReLU	16 ch, 9 k, ReLU	128 ch, 3 k, ReLU	64 ch, 9 k, ReLU	128 ch, 3 k, ReLU
Maxpooling	pool size: 2				
Dropout	10%				
Bachnormalization					
Conv(2D or 1D)	64 ch, 7 × 7 k, ReLU	32 ch, 7 k, ReLU	256 ch, 3 k, ReLU	128 ch, 7 k, ReLU	256 ch, 3 k, ReLU
Maxpooling	pool size: 2				
Dropout	10%				
Bachnormalization					
Conv(2D or 1D)	128 ch, 5 × 5 k, ReLU	64 ch, 5 k, ReLU	512 ch, 3 k, ReLU	256 ch, 5 k, ReLU	512 ch, 3 k, ReLU
Maxpooling	pool size: 2				
Dropout	10%				
Bachnormalization					
Conv(2D or 1D)	256 ch, 3 × 3 k, ReLU	128 ch, 3 k, ReLU	–	512 ch, 3 k, ReLU	–
Maxpooling	pool size: 2		–	pool size: 2	–
Dropout	10%		–	10%	–
Bachnormalization			–		–
Dense	1024 ch, Tanh	1024 ch, Tanh	1024 ch, Tanh	1024 ch, Tanh	1024 ch, Tanh
Dropout	30%				
Bachnormalization					
Dense	1 ch, Sigmoid	1 ch, Sigmoid	1 ch, Sigmoid	1 ch, Sigmoid	1 ch, Sigmoid

LSTM are designed to address the shortcoming of RNN when the sequence of data is large. They decide what information should be kept or discarded through their different gates to make accurate predictions.

All signals, here, are considered as time sequences, thus we use LSTM to find how they could learn the relations between input signals and the CDs. The architecture designed for this purpose is similar for all types of signals and summarized in Table 2. The main layer is a LSTM layer with 512 units, which is followed by a Dense layer with 1024 channels and a Bachnormalization layer. A Dropout layer with 30% is used after both LSTM and Dense layers. The CD value is predicted by a final Dense layer with 1 channel. In all layers ReLU is used as the activation function.

3. Results and discussion

Two types of ML methods (CNN and LSTM), with the mentioned architectures, were used for predicting CD values from five sets of data with various wl/cl ratios each with 1000 simulations. In each case, the transmitted and reflected waves and their following coda waves in two perpendicular (i.e. z- and x-) components were assume as the input data. All data were normalized into [0, 1]. We used soft-clipping normalization for the signals (Zhu et al., 2019):

$$S_n = \frac{1}{1 + e^{-kS_o}} \tag{3}$$

where S_o and S_n are original and normalized signals and k is chosen empirically based on the maximum amplitude in the original signal. Since CDs are in the range of [0.05, 0.4], they were simply multiplied by 2.5 to produce normalized outputs. All 1000 models (for each wl/cl) are divided into 75% and 25% as training and validation data, respectively. Since validation data are not seen by the network during the training phase, they were also used as test data. We used two popular criteria for evaluation of predictions namely MSE and coefficient of determination (R^2) with the following relations:

$$\mathrm{MSE} = \frac{1}{n}\sum_{i=1}^{n}\left(CD_i - \widehat{CD}_i\right)^2 \tag{4}$$

$$R^2 = 1 - \frac{SS_{\mathrm{res}}}{SS_{\mathrm{tot}}} \tag{5}$$

where CD and $\widehat{CD}$ are original and predicted CDs for n data. Also SS_{tot} and SS_{res} are the total and residual sum of squares errors regarding mean and predicted CDs, respectively.

To have a better arrangement, we divided the results into transmitted and reflected waves as follows and, in each part, we will discuss the capabilities of the ML methods.

3.1. Transmitted waves

Tables 3 and 4 are summaries of results obtained for transmitted waves in z- and x-components, respectively. These results reveal that both CNN and LSTM are valid enough to capture the highly complex relationship between input signals and output CDs. Since their accuracies are very close, it can be concluded that both of them are reliable methods for CD predictions.

According to Table 3, the best performance of the ML methods is in the case with wl/cl = 34. Although all cases are discussed in detail, here we examine this case as the best predictions. To have a better view of these results, Fig. 5 illustrates loss values and predictions for various methods and data of this case. Based on MSE and R^2 values in this figure, both CNN and LSTM produced promising predictions of CD either for 2D, 1D, or coda transmitted waves. In the following sub-sections, we will discuss them in detail.

Table 4 summarizes the results for the same model (wl/cl = 34), but for x-component signals. A comparison of these results with z-component (Table 3) demonstrates that the ML networks perform similarly as z-component data in this case. Our investigation showed that the same trends as x-component data are seen in z-component and, therefore, we avoid reporting similar results. Another reason for not going through x-component data is that they are not routine data in lab tests, and one may need special receivers to record signals in x-component.

Table 2
The architecture of the CNNs used in this study (ch: number of channels, ReLU: activation functions).

Input layer	All types of 1D-signlas
LSTM	512 units, ReLU
Dropout	30%
Dense	1024 ch, ReLU
Dropout	30%
Bachnormalization	
Dense	1 ch, ReLU

Table 3
ML results for prediction of CD from transmitted waves (z-component).

wl/cl	ML	Phase	Criterion	2D transmitted waves (z-comp)	1D transmitted waves (z-comp)	1D transmitted coda waves (z-comp)
0.64	CNN	Train	MSE (e-4)	10	4	10
			R^2 (%)	98.37	99.40	98.25
		Test	MSE (e-4)	40	46	192
			R^2 (%)	93.79	93.30	70.01
	LSTM	Train	MSE (e-4)	–	14	20
			R^2 (%)	–	97.8	96.88
		Test	MSE (e-4)	–	63	136
			R^2 (%)	–	90.8	77.8
2.5	CNN	Train	MSE (e-4)	4	4	3
			R^2 (%)	99.42	99.38	99.55
		Test	MSE (e-4)	8	12	63
			R^2 (%)	98.65	98.17	87.57
	LSTM	Train	MSE (e-4)	–	7	21
			R^2 (%)	–	98.82	96.63
		Test	MSE (e-4)	–	10	76
			R^2 (%)	–	98.30	86.66
8.5	CNN	Train	MSE (e-4)	2	4	2
			R^2 (%)	99.31	99.31	99.64
		Test	MSE (e-4)	4	5	29
			R^2 (%)	99.31	99.08	95.62
	LSTM	Train	MSE (e-4)	–	5	31
			R^2 (%)	–	99.17	94.90
		Test	MSE (e-4)	–	5	42
			R^2 (%)	–	99.28	93.54
34	CNN	Train	MSE (e-4)	**4**	**4**	**3**
			R^2 (%)	**99.36**	**99.44**	**99.52**
		Test	MSE (e-4)	**5**	**6**	**25**
			R^2 (%)	**99.24**	**99.02**	**96.31**
	LSTM	Train	MSE (e-4)	**–**	**4**	**10**
			R^2 (%)	**–**	**99.32**	**98.48**
		Test	MSE (e-4)	**–**	**9**	**20**
			R^2 (%)	**–**	**99.04**	**97.13**
136	CNN	Train	MSE (e-4)	11	10	17
			R^2 (%)	98.19	98.48	97.46
		Test	MSE (e-4)	11	16	74
			R^2 (%)	98.27	97.35	88.96
	LSTM	Train	MSE (e-4)	–	15	41
			R^2 (%)	–	97.72	93.42
		Test	MSE (e-4)	–	17	51
			R^2 (%)	–	97.22	92.36

Table 4
ML results for prediction of CD from transmitted waves (x-component).

wl/cl	ML	Phase	Criterion	2D transmitted waves (x-comp)	1D transmitted waves (x-comp)	1D transmitted coda waves (x-comp)
34	CNN	Train	MSE (e-4)	3	4	25
			R^2 (%)	99.49	99.42	99.09
		Test	MSE (e-4)	6	5	34
			R^2 (%)	99.08	99.29	94.93
	LSTM	Train	MSE (e-4)	–	3	45
			R^2 (%)	–	99.51	93.20
		Test	MSE (e-4)	–	3	50
			R^2 (%)	–	99.54	92.47

With our data set, it was possible to use both x- and z-components as the input data with two channels. However, our studies showed that no drastic improvement is seen regarding to what we have in each individual component. Therefore, we again avoid repeating similar results.

3.1.1. *Effect of wl/cl ratios*

As mentioned before, wl/cl ratio is one of the most important parameters in this study since it controls perturbation of the input signal which directly affects the CD predictions. In fact, one needs to use high frequency or low wavelength signal if micro-structure of rock such as pore, crack, and/or fracture are investigated. Nevertheless, the question is *how long should be signal wavelength to be used in the ML methods?* We generated numerical models for five sets of data with wl/cl of 0.64, 2.5, 8.5, 34, and 136 to explore this effect. Fig. 6 shows the variation of MSE and R^2 for various wl/cl for transmitted waves. Based on these plots, the optimum range could be introduced as $5 \leq$ wl/cl ≤ 50. The MSE and R^2 are minimum and maximum in the case of wl/cl = 34 as the best case in this study. By increasing wl/cl to 136, input signals are less affected by the cracks (see Fig. 4) leading to poorer predictions. Decreasing this ratio has the same effect, but this time it is due to strong effects of cracks which generate highly perturbed signals making the prediction process more complex. Experimentally speaking, using a normal transducer producing signals with 100–200 kHz frequencies, the ML methods can be applied for CD prediction for crack lengths about 0.75–1.5 mm.

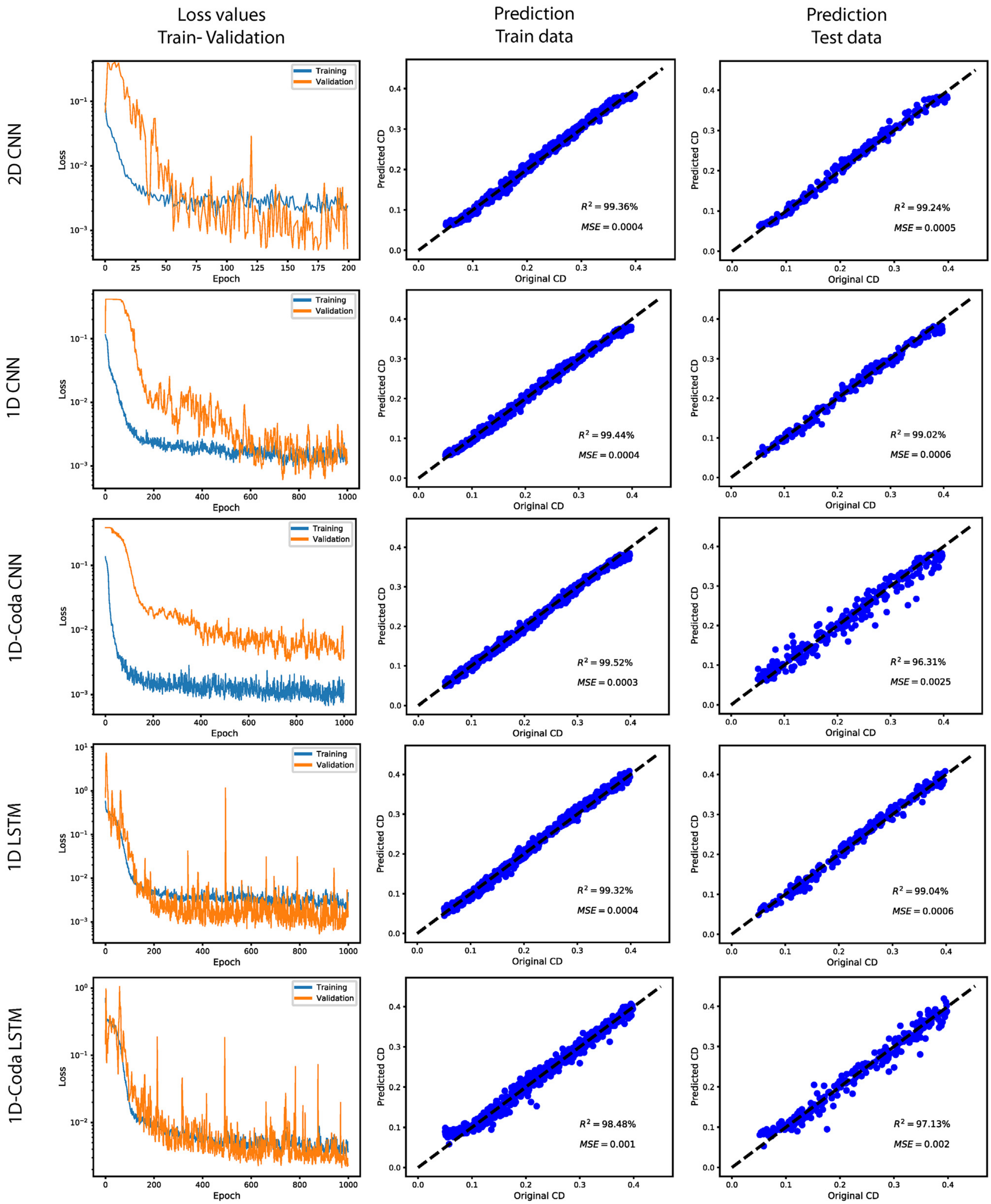

Fig. 5. Loss and prediction values of different methods (CNN, LSTM) for different phases (train, validation and test data) and different transmitted data (2D, 1D and coda) for the case of wl/cl = 34 as the best cases.

3.1.2. Comparison of 2D and 1D data

There are many successful applications of CNN with 2D input data (see Introduction). Here, we aim to evaluate such a capability for CD predictions. However, from a practical point of view, recording such a 2D section (t-x) is not straightforward and special receivers are needed. The conventional receivers in the laboratory or in the field (geophone) record just a 1D signal along the time and, therefore, these kinds of signals are more desired to be used as inputs for ML networks.

Fig. 7 illustrates MSE and R^2 values for CD predictions based on 2D and 1D input signals. As expected, predictions by 2D input sig-

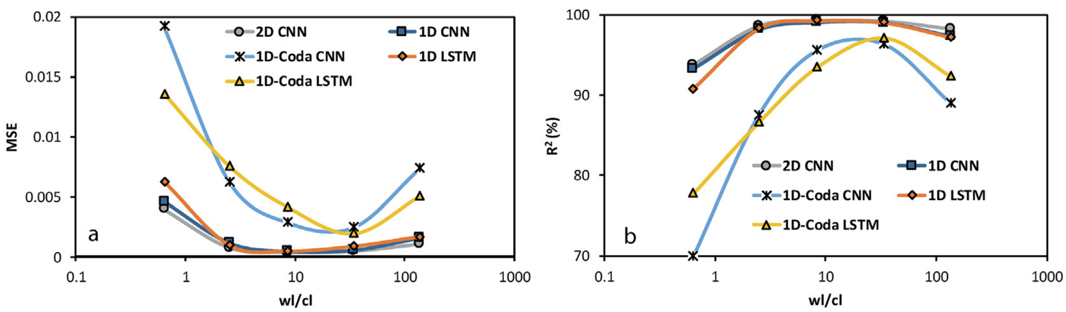

Fig. 6. The effect of wl/cl ratio on (a) MSE and (b) R^2 values of ML predictions.

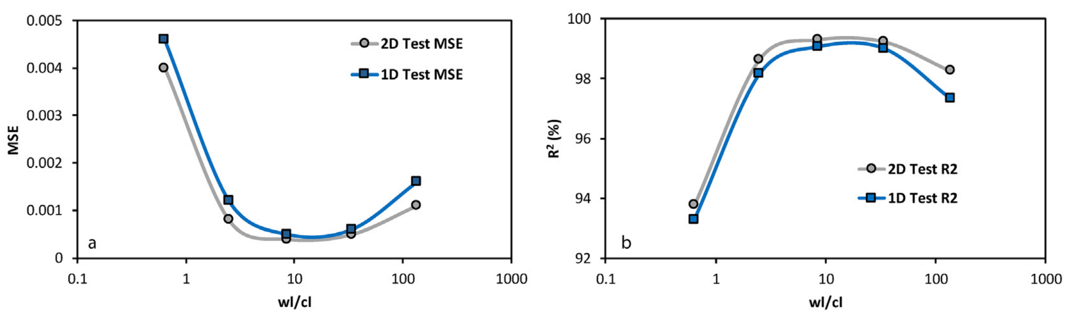

Fig. 7. (a) MSE and (b) R^2 (%) values of CNN for 2D and 1D signals.

nals are better. It is due to more features hidden in 2D signals, which a CNN can use them to find the relation between input and outputs much easier. However, with a slight difference, 1D signals produce someway the same accurate predictions although they contain less features relative to 2D signals. This means hidden features in 1D signals are informative enough to train a CNN for the purpose of CD prediction. This is an important result of this work since it demonstrates that even with the common receivers and 1D signals in the lab, the ML methods still could be trained to learn how to produce reliable predictions.

3.1.3. Comparison of 1D and 1D-coda signals

A powerful feature, which helps the ML methods to learn the relation between input signals and corresponding CDs, is the time of the first arrival signal (Figs. 2–4). Increasing CDs leads to decreasing effective elastic parameters and, therefore, lower wave velocity. Subsequently, longer arrival time for receiving first arrivals is needed. Even this small variation can be extracted by the ML methods. It is interesting to see what happens if we remove the first arrivals and train the networks with just coda signals.

Fig. 8 compares the accuracies of the CNN and LSTM for predicting CDs from 1D and their corresponding coda waves. As expected, removing first arrivals decreased the accuracy of predictions in both methods, however, they are still reasonable in the optimum range ($5 \le$ wl/cl ≤ 50). The MSE are lesser than 29e-4 and 42e-4 and R^2 values are higher than 95.62% and 93.54% for CNN and LSTM, respectively. These results are also promising since they indicate that the ML networks can be trained even if we miss the first arrivals in the data and just coda waves are available.

3.2. Reflected waves

Reflected waves are desired in many seismic applications as well as ultrasonic measurements. This study showed that the ML methods are proper choices for CD prediction using transmitted waves. However, the question is *how well CD predictions are if reflected waves are used as the input signals?* To this end and using a similar procedure as the previous section, we used the same ML architectures for the CNN and LSTM (Tables 1 and 2). Then, the ML networks were trained after normalizing and dividing data using the reflected signals. Tables 5 and 6 show the results for *z*- and *x*-components of reflected data for different wl/cl of 0.64, 2.5, 8.5, 34 and 134. Similar to the transmitted data, both CNN and LSTM could be an effective candidate ML method for CD predictions. The results of the case with wl/cl = 34 can be introduced again as the best case with the most reliable predictions. Fig. 9 shows the

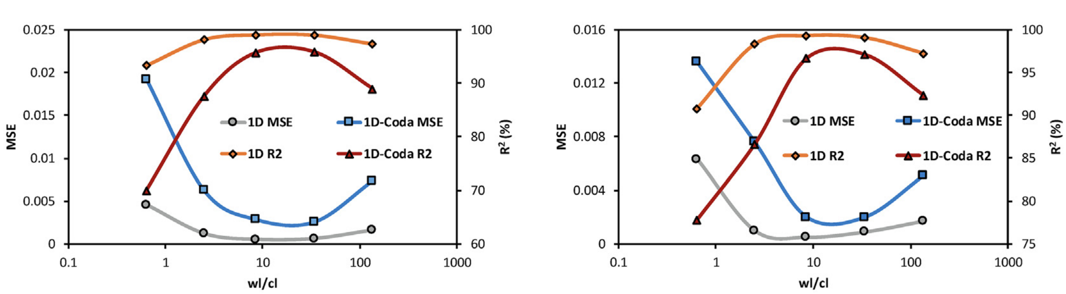

Fig. 8. (a) CNN and (b) LSTM performance for 1D and 1D-coda signals.

Table 5
ML results for prediction of CD from reflected waves.

wl/cl	ML	Phase	Criterion	1D transmitted waves	1D transmitted coda waves
0.64	CNN	Train	MSE (e-4)	4	9
			R^2 (%)	99.34	98.61
		Test	MSE (e-4)	168	209
			R^2 (%)	70.91	66.94
	LSTM	Train	MSE (e-4)	290	32
			R^2 (%)	97.55	95.08
		Test	MSE (e-4)	316	361
			R^2 (%)	50.33	45.31
2.5	CNN	Train	MSE (e-4)	4	2
			R^2 (%)	99.31	99.96
		Test	MSE (e-4)	83	80
			R^2 (%)	87.40	87.64
	LSTM	Train	MSE (e-4)	25	13
			R^2 (%)	95.81	97.79
		Test	MSE (e-4)	174	199
			R^2 (%)	73.38	68.20
8.5	CNN	Train	MSE (e-4)	6	5
			R^2 (%)	99.00	99.17
		Test	MSE (e-4)	25	29
			R^2 (%)	95.73	95.15
	LSTM	Train	MSE (e-4)	15	20
			R^2 (%)	97.48	96.74
		Test	MSE (e-4)	85	106
			R^2 (%)	86.46	83.45
34	CNN	Train	MSE (e-4)	**5**	**6**
			R^2 (%)	**99.25**	**99.11**
		Test	MSE (e-4)	**18**	**22**
			R^2 (%)	**97.11**	**96.70**
	LSTM	Train	MSE (e-4)	**8**	**18**
			R^2 (%)	**98.76**	**97.19**
		Test	MSE (e-4)	**22**	**42**
			R^2 (%)	**96.54**	**93.81**
136	CNN	Train	MSE (e-4)	45	55
			R^2 (%)	96.42	91.28
		Test	MSE (e-4)	43	70
			R^2 (%)	93.46	89.97
	LSTM	Train	MSE (e-4)	32	78
			R^2 (%)	94.20	88.32
		Test	MSE (e-4)	49	84
			R^2 (%)	91.50	85.88

Table 6
ML results for prediction of CD from reflected waves (*x*-component).

wl/cl	ML	Phase	Criterion	1D reflected waves (*x*-comp)	1D reflected coda waves (*x*-comp)
34	CNN	Train	MSE (e-4)	5	8
			R^2 (%)	99.18	98.74
		Test	MSE (e-4)	9	28
			R^2 (%)	98.59	95.62
	LSTM	Train	MSE (e-4)	5	22
			R^2 (%)	99.22	96.48
		Test	MSE (e-4)	12	46
			R^2 (%)	98.27	92.16

performance of the CNN and LSTM for this case, which are somehow comparable to each other. This emphasizes that we can candidate both methods for CD predictions. It is implied that these predictions are less accurate than those predicted by transmitted signals, however, MSE and R^2 values shows that they are promising results indicating that the ML methods can also be used for CD prediction even with reflected signals. This could be an interesting output for active/passive seismic applications, where reflected and/or coda waves are recorded.

Similar to the last section, we produced results for *x*-component of reflected signals (Table 4) with wl/cl = 34. It is observed that similar results relative to the *z*-component are obtained. Since other results and their trends are very similar to the *z*-component, we avoid repetition.

3.2.1. Effect of wl/cl ratio

To explore the effect of wl/cl on CD predictions from reflected signals, the same models with wl/cl = 0.64, 2.5, 8.5, 34, 136 were used. Fig. 10 illustrates these results as MSE and R^2 values. According to these plots, we can introduce $10 \leq$ wl/cl ≤ 100 as the optimum range and again the wl/cl = 34 as the best case. Other wl/cl values beyond this range lead to less accurate predictions, which we have discussed them in section 3.1.1.

3.2.2. Comparison of 1D and 1D-coda signals

As demonstrated, first arrivals could be a supportive feature steering prediction into the right values. However, it interesting to see how well predictions are using just coda waves. Fig. 11 shows some plots of MSE and R^2 values for 1D and 1D coda waves.

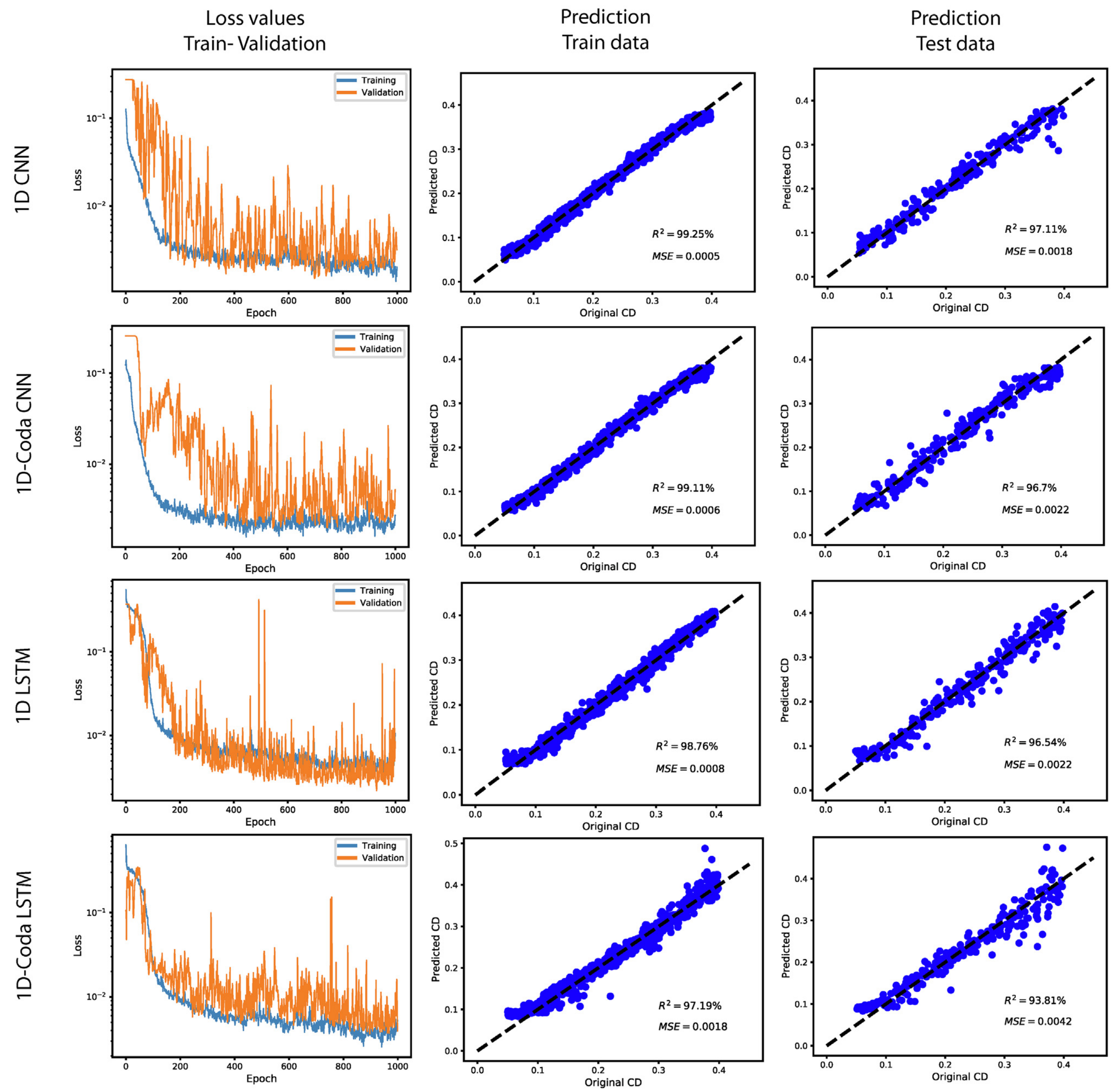

Fig. 9. Loss and prediction values of different methods (CNN, LSTM) for different phases (train, validation and test data) and different reflected data (1D and coda) for the case of wl/cl = 34 as one of the best cases.

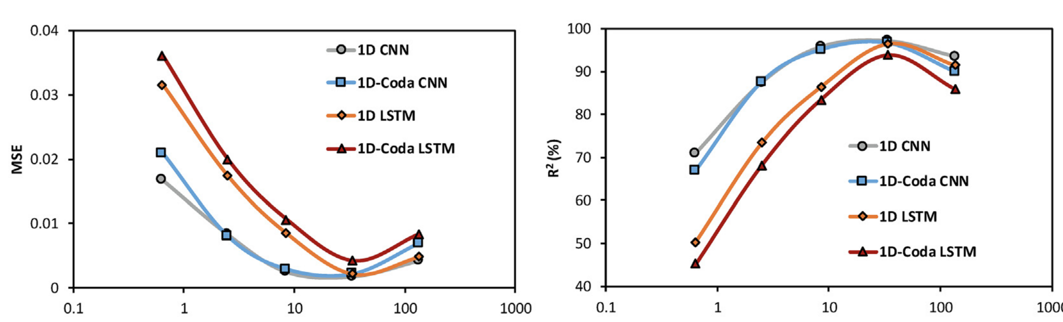

Fig. 10. The effect of wl/cl ratio on (a) MSE and (b) R^2 values of ML predictions.

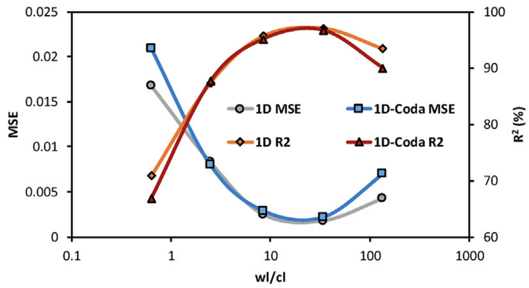

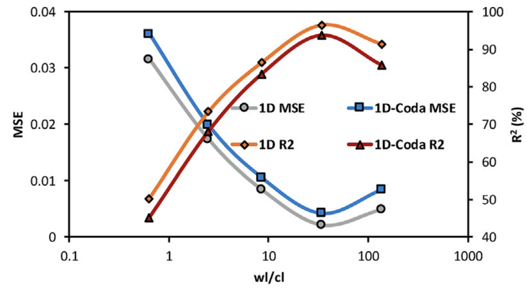

Fig. 11. (a) CNN and (b) LSTM performance for 1D and 1D-coda signals.

It implies that coda waves are less accurate, however, their differences are very small declaring that they could be used in such studies if wl/cl is selected in the optimum range.

4. Conclusions

In this study, the capabilities of the ML methods were investigated for the prediction of CD from waveform signal traversing through cracked models. These models were numerically generated with different values of CD. The background is a homogenous material and cracks are supposed to be in dry condition. A plane wave was propagated through the model using an RSG finite-difference method. By positioning two series of receiver lines at the top and bottom of the crack region, we recorded reflected and transmitted waves in both *x*- and *z*-component. Each series of receivers produces a 2D section of signals and we produced a 1D signal by averaging on all receivers in each section. Besides, by removing the first arrival high-amplitude signals, we also generated coda waves. All types of signals were generated for five wl/cl ratios of 0.64, 2.5, 8.5, 34, and 136 and 1000 models for each wl/cl. Each type of these signals was assumed as an individual input and was used to predict CD values.

The CNN and LSTM networks were used in this study. All signals were normalized using soft-clipping normalization and training-test data were divided by 75%–25%. Results showed that the accuracy of predictions for test data could reach R^2 > 96% with MSE < 25e-4. According to these results, we can conclude as follows:

(1) Both the CNN and LSTM networks are powerful enough to learn the complex relations between the input signals and CD values.
(2) There are optimum ranges to reach the best perditions, which are $5 \leq$ wl/cl ≤ 50 and $10 \leq$ wl/cl ≤ 100 for the transmitted and reflected signals, respectively.
(3) Both the transmitted and reflected signals are accurate enough. However, the accuracy of transmitted signals is slightly higher than the reflected signals.
(4) The 2D signals produce marginally better predictions than 1D signals. However, 1D signals are still valid enough to be used as they are more common to be recorded in reality.
(5) Signals in both components could be used for prediction as their accuracy are comparable. This implies that a conventional receiver could easily be used for such purposes.
(6) Although the accuracy of coda signals is less than the whole signals, they are still highly accurate (R^2 > 92%) in the best cases for transmitted and reflected signals and in both *x*- and *z*-component. This shows that the coda waves are still informative enough to be used as input data in the ML networks.

Declaration of Competing Interest

The authors declare that they have no known competing financial interests or personal relationships that could have appeared to influence the work reported in this paper.

Acknowledgements

EHS thanks the Deutsche Forschungsgemeinschaft (DFG) for financial support of the CODA-project (FOR 2825).

References

Aloysius, N., Geetha, M., 2018. A review on deep convolutional neural networks. In: Proceedings of the 2017 IEEE International Conference on Communication and Signal Processing, ICCSP 2017. Institute of Electrical and Electronics Engineers Inc, pp. 588–592. https://doi.org/10.1109/ICCSP.2017.8286426.

Ba, J., Xu, W., Fu, L.-Y., Carcione, J.M., Zhang, L., 2017. Rock anelasticity due to patchy saturation and fabric heterogeneity: a double double-porosity model of wave propagation. J. Geophys. Res. Solid Earth 122, 1949–1976. https://doi.org/10.1002/2016JB013882.

Bai, T., Tahmasebi, P., 2020. Hybrid geological modeling: combining machine learning and multiple-point statistics. Comput. Geosci. 142, 104519. https://doi.org/10.1016/j.cageo.2020.104519.

Bai, T., Tahmasebi, P., 2021. Efficient and data-driven prediction of water breakthrough in subsurface systems using deep long short-term memory machine learning. Comput. Geosci. 25, 285–297. https://doi.org/10.1007/s10596-020-10005-2.

Bayar, G., Bilir, T., 2019. A novel study for the estimation of crack propagation in concrete using machine learning algorithms. Constr. Build. Mater. 215, 670–685. https://doi.org/10.1016/J.CONBUILDMAT.2019.04.227.

Bernal, J., Kushibar, K., Asfaw, D.S., Valverde, S., Oliver, A., Martí, R., Lladó, X., 2019. Deep convolutional neural networks for brain image analysis on magnetic resonance imaging: a review. Artif. Intell. Med. 95, 64–81. https://doi.org/10.1016/j.artmed.2018.08.008.

Berryman, J.G., 1992. Single-scattering approximations for coefficients in Biots equations of poroelasticity. J. Acoust. Soc. Am. 91, 551–571. https://doi.org/10.1121/1.402518.

Bilir, T., Gencel, O., Topcu, I.B., 2016. Prediction of restrained shrinkage crack widths of slag mortar composites by Takagi and Sugeno ANFIS models. Neural Comput. Appl. 27, 2523–2536. https://doi.org/10.1007/s00521-015-2022-9.

Biot, M.A., 1962. Mechanics of deformation and acoustic propagation in porous media. J. Appl. Phys. 33, 1482–1498. https://doi.org/10.1063/1.1728759.

Biot, M.A., 1956. Theory of propagation of elastic waves in a fluid-saturated porous solid. I. Low-frequency range. J. Acoust. Soc. Am. 28, 168–178.

Blackshire, J.L., 2017. Enhanced damage characterization using wavefield imaging methods, in: AIP Conference Proceedings. American Institute of Physics Inc., p. 090008. https://doi.org/10.1063/1.4974652.

Budiansky, B., 1965. On the elastic moduli of some heterogeneous materials. J. Mech. Phys. Solids 13, 223–227. https://doi.org/10.1016/0022-5096(65)90011-6.

Byun, J.H., Lee, J.S., Park, K., Yoon, H.K., 2015. Prediction of crack density in porous-cracked rocks from elastic wave velocities. J. Appl. Geophys. 115, 110–119. https://doi.org/10.1016/j.jappgeo.2015.02.020.

Cai, M., Kaiser, P.K., Martin, C.D., 2001. Quantification of rock mass damage in underground excavations from microseismic event monitoring. Int. J. Rock Mech. Min. Sci. 38, 1135–1145. https://doi.org/10.1016/S1365-1609(01)00068-5.

Duan, X., Zhang, J., 2020. Multitrace first-break picking using an integrated seismic and machine learning method. Geophysics 85, WA269–WA277. https://doi.org/10.1190/geo2019-0422.1.

Gassmann, F., 1951. Elastic waves through a packing of spheres. Geophysics 16, 673–685.

Herraiz, M., Espinosa, A.F., 1987. Coda waves: a review. Pure Appl. Geophys. PAGEOPH 125, 499–577. https://doi.org/10.1007/BF00879572.
Hill, R., 1965. Continuum micro-mechanics of elastoplastic polycrystals. J. Mech. Phys. Solids 13, 89–101. https://doi.org/10.1016/0022-5096(65)90023-2.
Hochreiter, S., Schmidhuber, J., 1997. Long short-term memory. Neural Comput. 9, 1735–1780. https://doi.org/10.1162/neco.1997.9.8.1735.
Hoek, E., Martin, C.D., 2014. Fracture initiation and propagation in intact rock – a review. J. Rock Mech. Geotech. Eng. 6, 287–300. https://doi.org/10.1016/j.jrmge.2014.06.001.
Hou, B., Chang, Z., Fu, W., Muhadasi, Y., Chen, M., 2019. Fracture initiation and propagation in a deep shale gas reservoir subject to an alternating-fluid-injection hydraulic-fracturing treatment. SPE J. 24, 1839–1855. https://doi.org/10.2118/195571-PA.
Jing, L., Hudson, J.A., 2002. Numerical methods in rock mechanics. Int. J. Rock Mech. Min. Sci. 39, 409–427. https://doi.org/10.1016/S1365-1609(02)00065-5.
Kachanov, M., 1993. Elastic solids with many cracks and related problems. Adv. Appl. Mech. 30, 259–445. https://doi.org/10.1016/S0065-2156(08)70176-5.
Kachanov, M., 1992. Effective elastic properties of cracked solids: critical review of some basic concepts. Appl. Mech. Rev. 45, 304–336. https://doi.org/10.1115/1.3119761.
Kamali, A., Ghassemi, A., 2020. On the role of poroelasticity in the propagation mode of natural fractures in reservoir rocks. Rock Mech. Rock Eng. 53, 2419–2438. https://doi.org/10.1007/s00603-019-02017-x.
Kamrava, S., Tahmasebi, P., Sahimi, M., 2020. Linking morphology of porous media to their macroscopic permeability by deep learning. Transp. Porous Media 131, 427–448. https://doi.org/10.1007/s11242-019-01352-5.
Kamrava, S., Tahmasebi, P., Sahimi, M., 2019. Enhancing images of shale formations by a hybrid stochastic and deep learning algorithm. Neural Networks 118, 310–320. https://doi.org/10.1016/j.neunet.2019.07.009.
Karimpouli, S., Hassani, H., Malehmir, A., Nabi-Bidhendi, M., Khoshdel, H., 2013. Understanding the fracture role on hydrocarbon accumulation and distribution using seismic data: a case study on a carbonate reservoir from Iran. J. Appl. Geophys. 96, 98–106. https://doi.org/10.1016/j.jappgeo.2013.06.015.
Karimpouli, S., Tahmasebi, P., 2020. Physics informed machine learning: seismic wave equation. Geosci. Front. 11 (6), 1993–2001. https://doi.org/10.1016/j.gsf.2020.07.007.
Karimpouli, S., Tahmasebi, P., Ramandi, H.L., 2020a. A review of experimental and numerical modeling of digital coalbed methane: imaging, segmentation, fracture modeling and permeability prediction. Int. J. Coal Geol. 228, 103552. https://doi.org/10.1016/j.coal.2020.103552.
Karimpouli, S., Tahmasebi, P., Saenger, E.H., 2020b. Coal cleat/fracture segmentation using convolutional neural networks. Nat. Resour. Res. 29, 1675–1685. https://doi.org/10.1007/s11053-019-09536-y.
Kim, B.-C., Chen, J., Kim, J.-Y., 2020. Relation between crack density and acoustic nonlinearity in thermally damaged sandstone. Int. J. Rock Mech. Min. Sci. 125, 104171. https://doi.org/10.1016/j.ijrmms.2019.104171.
Kingma, D.P., Ba, J., 2014. Adam: A method for stochastic optimization. arXiv: 1412.6980v9.
Krizhevsky, A., Sutskever, I., Hinton, G.E., 2017. ImageNet classification with deep convolutional neural networks. Commun. ACM 60, 84–90. https://doi.org/10.1145/3065386.
Krüger, O.S., Saenger, E.H., Shapiro, S.A., 2005. Scattering and diffraction by a single crack: an accuracy analysis of the rotated staggered grid. Geophys. J. Int. 162, 25–31. https://doi.org/10.1111/j.1365-246X.2005.02647.x.
Lecun, Y., Bottou, L., Bengio, Y., Haffner, P., 1998. Gradient-based learning applied to document recognition. Proc. IEEE 86, 2278–2324. https://doi.org/10.1109/5.726791.
Mousavi, S.M., Ellsworth, W.L., Zhu, W., Chuang, L.Y., Beroza, G.C., 2020. Earthquake transformer—an attentive deep-learning model for simultaneous earthquake detection and phase picking. Nat. Commun. 11, 1–12. https://doi.org/10.1038/s41467-020-17591-w.
Nair, V., Hinton, G.E., 2010. Rectified Linear Units Improve Restricted Boltzmann Machines. BT - Proceedings of the 27th International Conference on Machine Learning (ICML-10), June 21-24, 2010, Haifa, Israel.
Nasirahmadi, A., Sturm, B., Edwards, S., Jeppsson, K.-H., Olsson, A.-C., Müller, S., Hensel, O., 2019. Deep learning and machine vision approaches for posture detection of individual pigs. Sensors 19 (17), 3738. https://doi.org/10.3390/s19173738.
Nasseri, M.H.B., Schubnel, A., Young, R.P., 2007. Coupled evolutions of fracture toughness and elastic wave velocities at high crack density in thermally treated Westerly granite. Int. J. Rock Mech. Min. Sci. 44, 601–616. https://doi.org/10.1016/j.ijrmms.2006.09.008.
Orlowsky, B., Saenger, E.H., Guéguen, Y., Shapiro, S.A., 2003. Effects of parallel crack distributions on effective elastic properties - A numerical study. Int. J. Fract. 124, L171–L178. https://doi.org/10.1023/B:FRAC.0000022563.29991.80.
Prasanna, P., Dana, K.J., Gucunski, N., Basily, B.B., La, H.M., Lim, R.S., Parvardeh, H., 2016. Automated crack detection on concrete bridges. IEEE Trans. Autom. Sci. Eng. 13, 591–599. https://doi.org/10.1109/TASE.2014.2354314.
Rezanezhad, M., Lajevardi, S.A., Karimpouli, S., 2019. Effects of pore-crack relative location on crack propagation in porous media using XFEM method. Theor. Appl. Fract. Mech. 103, 102241. https://doi.org/10.1016/j.tafmec.2019.102241.
Saenger, E.H., Finger, C., Karimpouli, S., Tahmasebi, P., 2021. Single-station coda wave interferometry: a feasibility study using machine learning. Mater 14 (13), 3451. https://doi.org/10.3390/MA14133451.
Saenger, E.H., Gold, N., Shapiro, S.A., 2000. Modeling the propagation of elastic waves using a modified finite-difference grid. Wave Motion 31, 77–92. https://doi.org/10.1016/S0165-2125(99)00023-2.
Saenger, E.H., Kruger, O.S., Shapiro, S.A., Krüger, O.S., Shapiro, S.A., 2004. Effective elastic properties of randomly fractured soils: 3D numerical experiments. Geophys. Prospect. 52, 183–195. https://doi.org/10.1111/j.1365-2478.2004.00407.x.
Saenger, E.H., Shapiro, S.A., 2002. Effective velocities in fractured media: a numerical study using the rotated staggered finite-difference grid. Geophys. Prospect. 50, 183–194. https://doi.org/10.1046/j.1365-2478.2002.00309.x.
Schubnel, A., Benson, P.M., Thompson, B.D., Hazzard, J.F., Young, R.P., 2006. Quantifying damage, saturation and anisotropy in cracked rocks by inverting elastic wave velocities. In: Dresen, G., Zang, A., Stephansson, O. (Eds.), Rock Damage and Fluid Transport, Part I. Birkhäuser, Basel, pp. 947–973. https://doi.org/10.1007/3-7643-7712-7_3.
Tahmasebi, P., Kamrava, S., Bai, T., Sahimi, M., 2020. Machine learning in geo- and environmental sciences: from small to large scale. Adv. Water Resour. 142, 103619. https://doi.org/10.1016/j.advwatres.2020.103619.
Tang, S., Wang, J., Tang, C., 2021. Identification of microseismic events in rock engineering by a convolutional neural network combined with an attention mechanism. Rock Mech. Rock Eng. 54 (1), 47–69. https://doi.org/10.1007/s00603-020-02259-0.
Thomsen, L., 1985. Biot-consistent elastic moduli of porous rocks: low-frequency limit. Geophysics 50 (12), 2797–2807. https://doi.org/10.1190/1.1441900.
van der Voet, E., Muchez, P., Laenen, B., Weltje, G.J., Lagrou, D., Swennen, R., 2020. Characterizing carbonate reservoir fracturing from borehole data – a case study of the Viséan in northern Belgium. Mar. Pet. Geol. 111, 375–389. https://doi.org/10.1016/j.marpetgeo.2019.08.040.
Waldeland, A.U., Jensen, A.C., Gelius, L.-J., Solberg, A.H.S., 2018. Convolutional neural networks for automated seismic interpretation. Lead. Edge 37, 529–537. https://doi.org/10.1190/tle37070529.1.
Xiong, W., Ji, X.u., Ma, Y., Wang, Y., AlBinHassan, N.M., Ali, M.N., Luo, Y.i., 2018. Seismic fault detection with convolutional neural network. Geophysics 83, O97–O103. https://doi.org/10.1190/geo2017-0666.1.
Yoon, H.-K., 2020. Relationship between aspect ratio and crack density in porous-cracked rocks using experimental and optimization methods. Appl. Sci. 10, 7147. https://doi.org/10.3390/app10207147.
Yu, Y., Si, X., Hu, C., Zhang, J., 2019. A review of recurrent neural networks: Lstm cells and network architectures. Neural Comput. 31, 1235–1270. https://doi.org/10.1162/neco_a_01199.
Zhang, L., Ba, J., Carcione, J.M., Fu, L., yun, 2020. Differential poroelasticity model for wave dissipation in self-similar rocks. Int. J. Rock Mech. Min. Sci. 128,. https://doi.org/10.1016/J.IJRMMS.2020.104281 104281.
Zhang, L., Ba, J., Carcione, J.M., Sun, W., 2019. Modeling wave propagation in cracked porous media with penny-shaped inclusions. Geophysics 84, WA141–WA151. https://doi.org/10.1190/geo2018-0487.1.
Zhang, X., Zhang, M., Tian, X., 2021a. Real-time earthquake early warning with deep learning: Application to the 2016 Central Apennines, Italy Earthquake Sequence. Geophys. Res. Lett. 48(5), article id. e9394.
Zhang, Y., Chan, W., Jaitly, N., 2017. Very deep convolutional networks for end-to-end speech recognition. In: in: 2017 IEEE International Conference on Acoustics, Speech and Signal Processing (ICASSP). IEEE, pp. 4845–4849. https://doi.org/10.1109/ICASSP.2017.7953077.
Zhang, Z.X., Chi, L.Y., Qiao, Y., Hou, D.F., 2021b. Fracture initiation, gas ejection, and strain waves measured on specimen surfaces in model rock blasting. Rock Mech. Rock Eng. 54, 647–663. https://doi.org/10.1007/s00603-020-02300-2.
Zhu, L., Peng, Z., McClellan, J., Li, C., Yao, D., Li, Z., Fang, L., 2019. Deep learning for seismic phase detection and picking in the aftershock zone of 2008 Mw7.9 Wenchuan Earthquake. Phys. Earth Planet. Inter. 293,. https://doi.org/10.1016/j.pepi.2019.05.004 106261.
Zhuang, L., Kim, K.Y., Diaz, M., Yeom, S., 2020. Evaluation of water saturation effect on mechanical properties and hydraulic fracturing behavior of granite. Int. J. Rock Mech. Min. Sci. 130, 104321. https://doi.org/10.1016/j.ijrmms.2020.104321.